Biosensors and Bioelectronics 81 (2016) 388–394

Contents lists available at ScienceDirect

Biosensors and Bioelectronics

journal homepage: www.elsevier.com/locate/bios

Label-free DNA biosensor based on resistance change of platinum nanoparticles assemblies

Evangelos Skotadis [a,*], Konstantinos Voutyras [a], Marianneza Chatzipetrou [a], Georgios Tsekenis [b], Lampros Patsiouras [a], Leonidas Madianos [a], Stavros Chatzandroulis [c], Ioanna Zergioti [a], Dimitris Tsoukalas [a,*]

[a] Department of Applied Physics, National Technical University of Athens, Athens 15780, Greece
[b] Biomedical Research Foundation of the Academy of Athens, Athens 11527, Greece
[c] Institute of Nanoscience and Nanotechnology NCSR Demokritos, Athens 60228, Greece

ARTICLE INFO

Article history:
Received 23 December 2015
Received in revised form
24 February 2016
Accepted 14 March 2016
Available online 15 March 2016

Keywords:
Platinum nanoparticles
Sputtering
Resistance
Biosensor
Electrochemical
DNA

ABSTRACT

A novel nanoparticle based biosensor for the fast and simple detection of DNA hybridization events is presented. The sensor utilizes hybridized DNA's charge transport properties, combining them with metallic nanoparticle networks that act as nano-gapped electrodes. The DNA hybridization events can be detected by a significant reduction in the sensor's resistance due to the conductive bridging offered by hybridized DNA. By modifying the nanoparticle surface coverage, which can be controlled experimentally being a function of deposition time, and the structural properties of the electrodes, an optimized biosensor for the in situ detection of DNA hybridization events is ultimately fabricated. The fabricated biosensor exhibits a wide response range, covering four orders of magnitude, a limit of detection of 1 nM and can detect a single base pair mismatch between probe and complementary DNA.

1. Introduction

The main goal of all current bio-sensing systems lies in the label free detection of bio-recognition events. For the successful development of such a system it is essential that the sensor can actually facilitate the formation of the probe-target complex (Drummond et al., 2003), triggering a measurable electrical signal. In a typical bio-recognition process a single stranded (ss) DNA sequence (probe molecule) is immobilized onto the functionalized surface of the sensor. A second DNA sequence (target molecule) is then recognized via the base-pair interactions between complementary sequences.

In the field of electrochemical biosensors in particular, there are many proposed technologies for the detection of probe-target hybridization events such as direct DNA electrochemical sensors (Li et al., 2016; Palecek, 1960, 1988; Singhal and Kuhr, 1997), indirect DNA electrochemical sensors (Armistead and Thorp, 2002; Yang and Thorp, 2001; Yang et al., 2002), DNA specific redox indicator detection sensors (Fojta et al., 2003; Malecka et al., 2016; Palecek et al., 2002; Umek et al., 2001), DNA mediated charge transport sensors (Boon and Barton, 2002; Furst et al., 2014; Kelley et al., 1997, 1999) as well as several strategies for the electrochemical amplification of the sensor read-out signal (Fang et al., 2008a, 2008b; Merkoçi, 2010).

Nanoparticle-based technologies have been also used for the development of bio-sensing systems for quite some time now (Ling et al., 2016; Merkoçi, 2010). In a nanoparticle based system events such as the recognition of a specific oligonucleotide sequence to an already immobilized DNA strand or antigen/antibody reactions, can induce significant changes in the optical and electrochemical properties of the system (Ahn et al., 2011; Gao et al., 2011; Lee et al., 2008; Wang et al., 2015). Metallic and semiconducting nanoparticles are of special interest and widely used in bio-sensing applications while the detection of any biological event can be achieved by monitoring changes in the impedance, potential and resistance of the device.

In a fairly different and radically new approach, compared to typical nanoparticle-based DNA electrochemical sensing systems, gold nanoparticles have been employed as nano-gapped electrodes for the detection of DNA hybridization events (Tokonami et al., 2008). Such a bio-sensing system is advantageous as there is no need for special tags that are activated in redox reactions during

* Corresponding authors.
E-mail addresses: evskotad@central.ntua.gr (E. Skotadis), dtsouk@central.ntua.gr (D. Tsoukalas).

http://dx.doi.org/10.1016/j.bios.2016.03.028
0956-5663/

the hybridization events (Lin et al., 2007). In this case, the substrates/electrodes are chemically modified to attract nanoparticles that are dispersed in solution while the final inter-nanoparticle distance is controlled by the chain length of the dithiol molecules. Following deposition and immobilization of probe ssDNA, the hybridization of complementary DNA target molecules can be monitored through the change induced in the conductivity/resistance of the nanoparticle film. This comes as no surprise since double-stranded (ds) DNA duplexes have been extensively studied over the last two decades for their charge transport properties (Dekker and Ratner, 2001; Giese, 2000; Okahata et al., 1998; Porath et al., 2000; Qi et al., 2015). In fact, in most studies the conductivity between consecutive or distanced DNA base pairs (charge transport has been observed even between distinctive base pairs having a distance of 40 base pairs to each other) is attributed to quantum mechanical tunneling (Giese, 2000). All of the above studies conclude that DNA strands can conduct electric current, when properly oriented, acting as conductive molecular linkers or as conductive "bridges" between metallic electrodes.

In the present article, the use of platinum nanoparticle networks of varying surface coverage has been implemented towards the development and optimization of an electrochemical bio sensing device for the highly specific, label free and fast in situ detection of DNA hybridization. Platinum nanoparticles, produced via a modified magnetron sputtering technique, detect a DNA hybridization event via a drop in the resistance of the device while the performance of the sensor can be optimized by the nanoparticle surface density and inter-finger electrode spacing. The sputtering method provides high flexibility, since it is fully compatible with semiconductor manufacturing technology/batch fabrication, the target material (in this case platinum) can be easily changed and the physically produced nanoparticles can self-assemble on top of silicon dioxide substrates without the need for a functionalization layer. As it has been previously shown by this group, platinum nanoparticle films can be successfully used as chemical or strain sensors (Skotadis et al., 2012, 2013; Tanner et al., 2012). By using a similar sensor design a simple, fast and highly responsive electrochemical biosensor for the detection of DNA hybridization events has been developed. The sensor is able to discern even between single base pair mismatches in DNA molecules and is characterized by a much simpler fabrication procedure, when compared to similar sensing systems (Tokonami et al., 2008). The current results expand the application range of our nanoparticle based multi-sensing platform, in the field of bio sensing.

2. Material and methods

All fabrication experiments were conducted at room temperature. All reagents were obtained from Aldrich Chemicals. All solutions were prepared with deionized water (18 MΩ/cm resistivity) from a Millipore MilliQ system. Silicon wafers with a thermal oxide layer of 50 nm, were used as deposition substrates throughout the experiments. Using conventional optical lithography, interdigitated electrodes (IDEs) were patterned on top of the oxidized silicon substrates (Fig. 1). By employing the e-gun evaporation technique, a Titanium layer of 3–5 nm in thickness was deposited to act as an adhesion layer between gold and the SiO_2 substrate. This was followed by gold deposition which formed electrodes with a thickness of no more than 50 nm after lift-off. The interdigitated electrodes inter finger distance (or electrode gap) varied between 30 μm, 10 μm and 5 μm.

Following electrode fabrication, platinum nanoparticles having a mean diameter of 4–6 nm and a mean surface roughness of 4.5 ± 0.5 nm (as calculated by atomic force microscopy) were

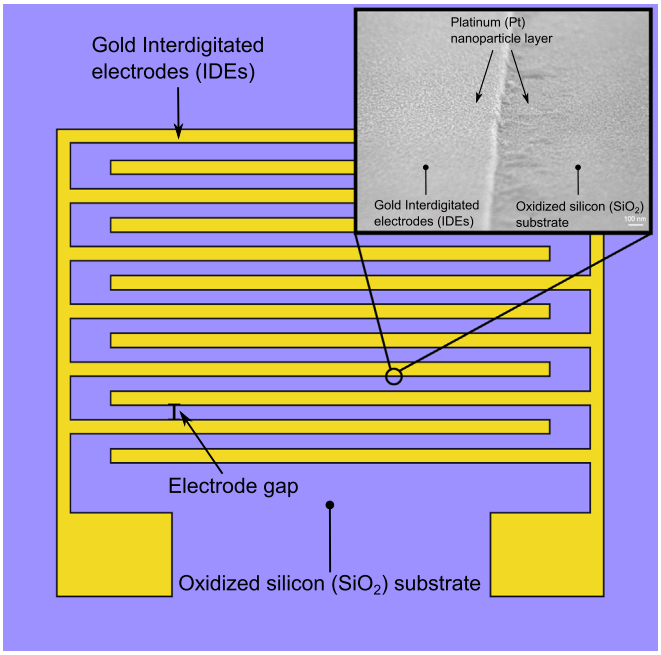

Fig. 1. Schematic of the gold interdigitated electrodes (IDEs) used throughout all experiments. Inset figure: Inclined SEM image (at an angle of 72°) of the platinum nanoparticle layer covering both the SiO_2 substrate and the gold IDEs.

deposited on top of the silicon substrates using a modified magnetron sputtering system (Fig. 1). Sputtering allows control over particle size (by adjusting the target material to deposition substrate distance), nanoparticle flux (by adjusting the argon flux and the acceleration voltage value, while monitoring it through a quartz crystal microbalance) and nanoparticle concentration on the substrate surface (time dependent). The resistance of the devices during the nanoparticle deposition was monitored in-situ and the deposition was interrupted as soon as the desired device resistance was achieved. Following nanoparticle deposition, the substrates were functionalized with 3-glycidyloxypropyltriethoxysilane (GOPTS), a silane bearing epoxy moieties, in order to enhance the binding of thiol-modified ssDNA probes (Tsekenis et al., 2012).

DNA oligonucleotides were purchased from Eurofins MWG Operon (Ebersberg, Germany) and their sequences are as follows: [ThiC6] – 5′-GTT GAC CTG GTC GTC-3′-FAM (fully complementary probe molecule), 5′-GAC GAC CAG GTC AAC-3′ (target molecule), [ThiC6] – 5′-TAG CCG ATA TGC GCA-3′-FAM (non complementary probe molecule) and 5′-HS-(CH2)6-TAG CCG AGA TGC GCA-3′-FAM (single base pare mismatch probe molecule). The physical length of these DNA sequences was about 6–7 nm for ssDNA. Hybridized target oligomers to immobilized probe DNA presents slightly decreased length due to the double helical nature of double stranded (ds) DNA, induced by the coiling of the DNA strands (5–6 nm). The ssDNA probe molecules, which were fully complementary (FC), bearing a single base pair mismatch (1MM) or non-complementary (NC) to the target DNA sequence, were deposited on top of the functionalized substrate entirely covering the surface of the IDEs. The ssDNA probes contained a 5′-thiol C6 linker and were labelled with (6-carboxyfluorescein) 6-FAM at the 3′ end. The target DNA sequence was tagged with Texas Red at the 5′ end. DNA deposition and hybridization were performed from a 1.0 M potassium phosphate buffer, 0.5 M KH_2PO_4 and 0.5 M K_2HPO_4 (pH 8) (Buffer 1). A wash buffer (10 mM NaCl, 5 mM Tris buffer, pH 7.4) was used to remove unbound probes or target ssDNA.

For the deposition of the ssDNA probes (both FC, 1MM and NC) the Laser Induced Forward Transfer technique (LIFT) was used

(Boutopoulos et al., 2011). The ssDNA probes were left to bind with the GOPTS-functionalized surfaces overnight at room temperature in phosphate buffer. Following immobilization the substrates were rinsed twice with Wash buffer and were subsequently exposed to a solution of 6-Mercapto-1-hexanol (MCH, used in a 1.0 mM solution in deionized water) for 1 h to remove any non-specifically bound molecules. Excess MCH was removed once again by rinsing the substrates twice with Wash buffer. Hybridization with the complementary sequence was achieved by incubating the surfaces at room temperature, with an excess of target DNA in phosphate buffer (5 μL were used to cover the entire active surface of the IDEs). The successful selective attachment of ss probe DNA on the surfaces, as well as their hybridization with target DNA was verified by fluorescence microscopy.

The devices were characterized by optical microscopy measurements, transmission electron microscopy (TEM) and field emission scanning electron microscopy (FE-SEM). Electrical characterization measurements were performed using the HP4140B picoampere meter.The fabricated prototype sensors were tested by in situ resistance measurements upon FC and NC probe to target DNA hybridization. Performance evaluation experiments were conducted at room temperature. The resistance of multiple sensors (up to 8 sensors can be measured simultaneously) was monitored in situ using a Keithley 2400 Multimeter and a custom-made multiplexer switch board. The measurement system was controlled via a PC and a custom-made software application. In order to ensure that any change in the measured resistance was solely due to target recognition by the immobilized probe ssDNA, 2 μL of buffer (1) were added on top of the IDEs until the system reached a steady-state. Before the addition of any target ssDNA, a further 2 μL of buffer (1) were added on top of the IDEs to ensure that the equilibrium state was not distorted. If the addition of buffer (1) shifted the measured resistance, additional buffer was applied to the system until equilibrium was reached once again (Fig. 2). Control experiments were also conducted, where any change in the resistance due to the interaction of a NC probe with the target molecule was quantified and subtracted from the specific response.

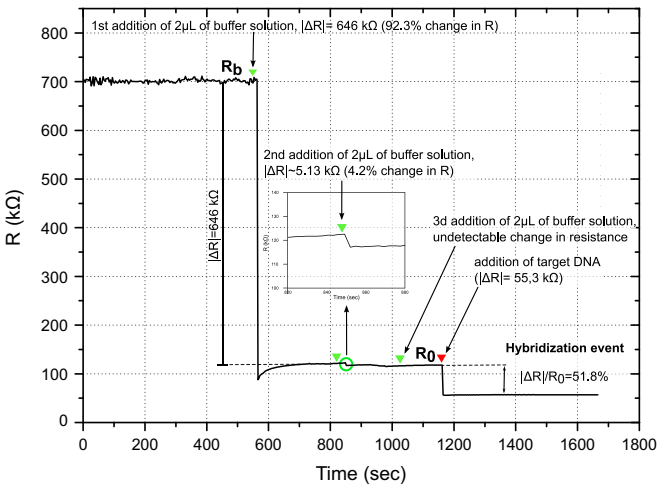

Fig. 2. Transient response of a nanoparticle based electrochemical biosensor (nanoparticle surface coverage: 46%, R_b: 700 kΩ and electrode gap: 5 μm). The response of the sensor, in terms of change in resistance, for repeated additions of buffer solution and finally for a fully complementary (FC) probe to target DNA hybridization event (target DNA concentration of 10 μM), can be seen.

3. Results and discussion

3.1. Sensing mechanism

Nanoparticle films prepared by the gas phase condensation of sputtered platinum atoms do not produce surfaces where the particles are self-organized in a periodic and repeatable manner (as in the case of a chemically modified surface) since the nanoparticles self-assemble on the substrate. This, however, does not mean that the nanoparticle surface distribution is random, due to the fact that the nanoparticles tend to aggregate and to form clusters. As the deposition time is extended more nanoparticles aggregate on these clusters, thus increasing the available conductive paths within the nanoparticle film and reducing its resistance. In fact, the conductivity of devices fabricated using the sputtering technique can fall in one of the three following conductivity states (Abeles et al., 1975): (i) the insulating state, where the individual nanoparticle nucleation centers are sufficiently distanced/isolated from each other and do not facilitate any charge transport; (ii) the quasi macroscopic state, where a high nanoparticle surface coverage forces individual aggregation centers to merge, thus forming “continuous” charge transport pathways; and (iii) the intermediate transition state where the conductivity of the device is in between the previous two states. The limit above which the conductivity transcends from the intermediate state to the quasi macroscopic state is the percolation threshold (Scher and Zallen, 1970).

The conductivity (σ) in this network of metallic nanoparticles can be adequately described in the context of a thermally activated tunneling mechanism expressed in the following manner (Neugebauer and Webb, 1962; Wang et al., 2007):

$$\sigma = \sigma_0 \exp(-\beta d)\exp(-E_A/k_B T) \quad (1)$$

where σ_0 is a pre-exponential constant, β is the electron coupling term, d is the inter-particle distance and k_B and T are the Boltzmann constant and temperature respectively. E_A is the activation energy which is given using the following relation:

$$E_A = 0.5e^2[r^{-1} - (r + d)^{-1}]/(4\pi\epsilon_r\epsilon_0) \quad (2)$$

where r is the nanoparticle radius, ε_0 is the dielectric constant and ε_r is the relative permittivity.

In results previously published by our research group (Skotadis et al., 2012, 2013; Tanner et al., 2012), it has been determined that there is an optimal nanoparticle surface coverage, which in turn translates in a corresponding device conductivity or resistance, that best serves the performance of a sensing device. In fact, optimal nanoparticle surface coverage was established to be in the range of 42–46% (or in the range of 600 kΩ to 1–10 MΩ for device resistance) which is substantially close to the critical density for percolation processes in a 2-D film according to Scher and Zallen, 1970. Devices whose conductivity lies just below the percolation threshold present increased sensing performance. By the in-situ monitoring of the resistance of a device the nanoparticle deposition can be interrupted just below the percolation threshold (device resistance in the range of 600 kΩ to 1–10 MΩ).

In the present paper, such nanoparticle-based sensors of varying conductivity were used as electrochemical biosensors. As further discussed below, the presence of hybridized DNA chains induces a change in the resistance/conductivity of the sensor if these DNA chains are allowed to act as conductive bridges between discrete nanoparticles or nanoparticles clusters, forming new high conductivity charge transport/percolation pathways.

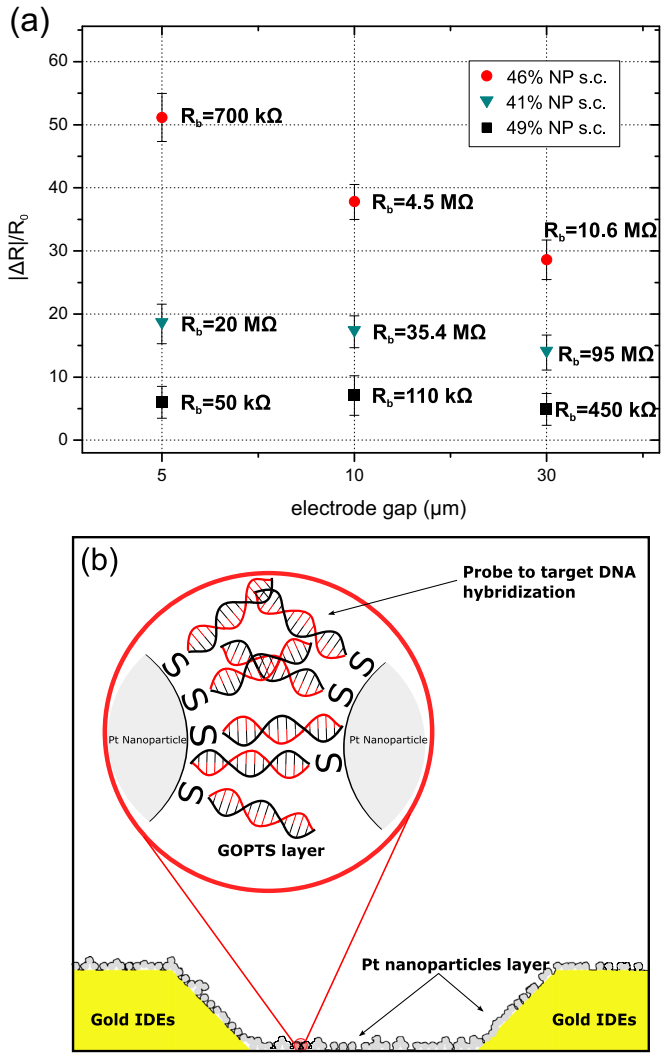

Fig. 3. Sensor response for target (10 μM in concentration) to probe (10 μM in concentration) DNA hybridization. (a) Relative resistance response ($|\Delta R|/R_0$) of all three sensor groups for target to fully complementary (FC) probe DNA hybridization (b) Cross section of the sensing device (schematic) after the target to probe DNA hybridization event.

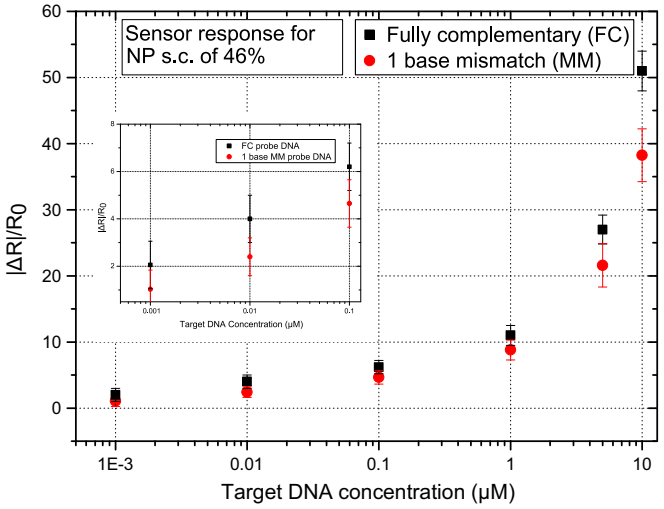

Fig. 4. Sensor response (nanoparticle surface coverage: 46%, IDE gap: 5 μm) for fully complementary (FC) probe to target DNA and single base pair mismatched (1 base MM) probe to target DNA hybridization, in a logarithmic scale.

3.2. Sensing results

3.2.1. Sensor optimization

By modifying the nanoparticle deposition time, 3 different sensor groups of varying nanoparticle surface coverage (hence resistance) were prepared. The nanoparticle surface coverage for each sensor group has been calculated using TEM images and an image processing software tool (imageJ). Using imageJ's inherent standard deviation routine, we have determined that a 2–3% standard deviation exists in all reported nanoparticle surface coverages. Also a difference of up to 2% exists in the NP surface coverage between sensors fabricated after different nanoparticle depositions but with the same resistance.

Furthermore and in order to demonstrate the increased sensitivity offered by reduced electrode inter-finger spacing (Ancona et al., 2006; Wang et al., 2006), three different electrode gaps (30 μm, 10 μm and 5 μm) were used throughout the experiments. The mean base resistances, or R_b (R_b: initial device resistance prior to any buffer or DNA addition, as seen in Fig. 2) following the same nanoparticle deposition for the first sensor group (nanoparticle surface coverage of 49%), were 50 kΩ for a 5 μm electrode gap, 110 kΩ for a 10 μm electrode gap and 450 kΩ for a 30 μm electrode gap. For the second sensor group (nanoparticle surface coverage of 46%) resistance values of 700 kΩ, 4.5 MΩ and 10.6 MΩ were obtained for 5 μm, 10 μm and 30 μm electrode gaps respectively (again for the same nanoparticle deposition). Finally, the third sensor group (nanoparticle surface coverage of 41%) had base resistances of 20 MΩ, 35.4 MΩ and 95 MΩ; for 5 μm, 10 μm and 30 μm electrode gaps respectively. Each of the three sensor groups comprised of 6 distinctive sensors for every electrode gap. The mean base resistance for every sensor group and its three respective electrode gaps had a standard deviation between 2% and 4%. For the detection of 10 μM of target DNA, 18 DNA biosensors have been used in total (6 for every distinctive electrode gap) for every sensor group. The standard deviation of these measurements varied from 1% to 3% as can be seen in Fig. 3(a). All sensors' resistances have been measured in a −1 to 1 V range. Sensors with a 5 μm electrode gap and resistances that fall in the several MΩ regime [insulating conductivity state (Tanner et al., 2012), nanoparticle surface coverage < 32%] or in the few hundred Ω regime [metallic conductivity state (Tanner et al., 2012], nanoparticle surface coverage > 50%) have been also tried as potential biosensors, but without any measurable change in sensor resistance upon probe to target DNA hybridization, as shall be explained below, in paragraph 3.2.3.

In Fig. 3(a), the response of the sensors following DNA hybridization was recorded as relative change in device resistance ($|\Delta R|/R_0$ where R_0 is the resistance of the sensor just before the DNA hybridization event, as can be seen in Fig. 2). The sensors respond with a decrease in resistance upon target (10 μM in concentration) to probe DNA (10 μM in concentration) hybridization, in agreement with what has already been reported (Tokonami et al., 2008), while sensors exhibiting conductivity/resistance just before the percolation threshold (nanoparticle surface coverage of 46%) outmatch their counterparts in terms of sensing response. Finally, the sensors have a fast response time of 10–15 s (Response time is the time needed for the sensor to reach 70% of equilibrium state).

The decrease in resistance observed during DNA hybridization is to be expected since hybridized DNA has been known to act as a molecular linker between conductive islands bridging any physical gaps [Fig. 3(b)]; therefore enhancing the overall conductivity of the device (Dekker and Ratner, 2001; Giese, 2000; Okahata et al., 1998; Porath et al., 2000). Finally the response of the "control

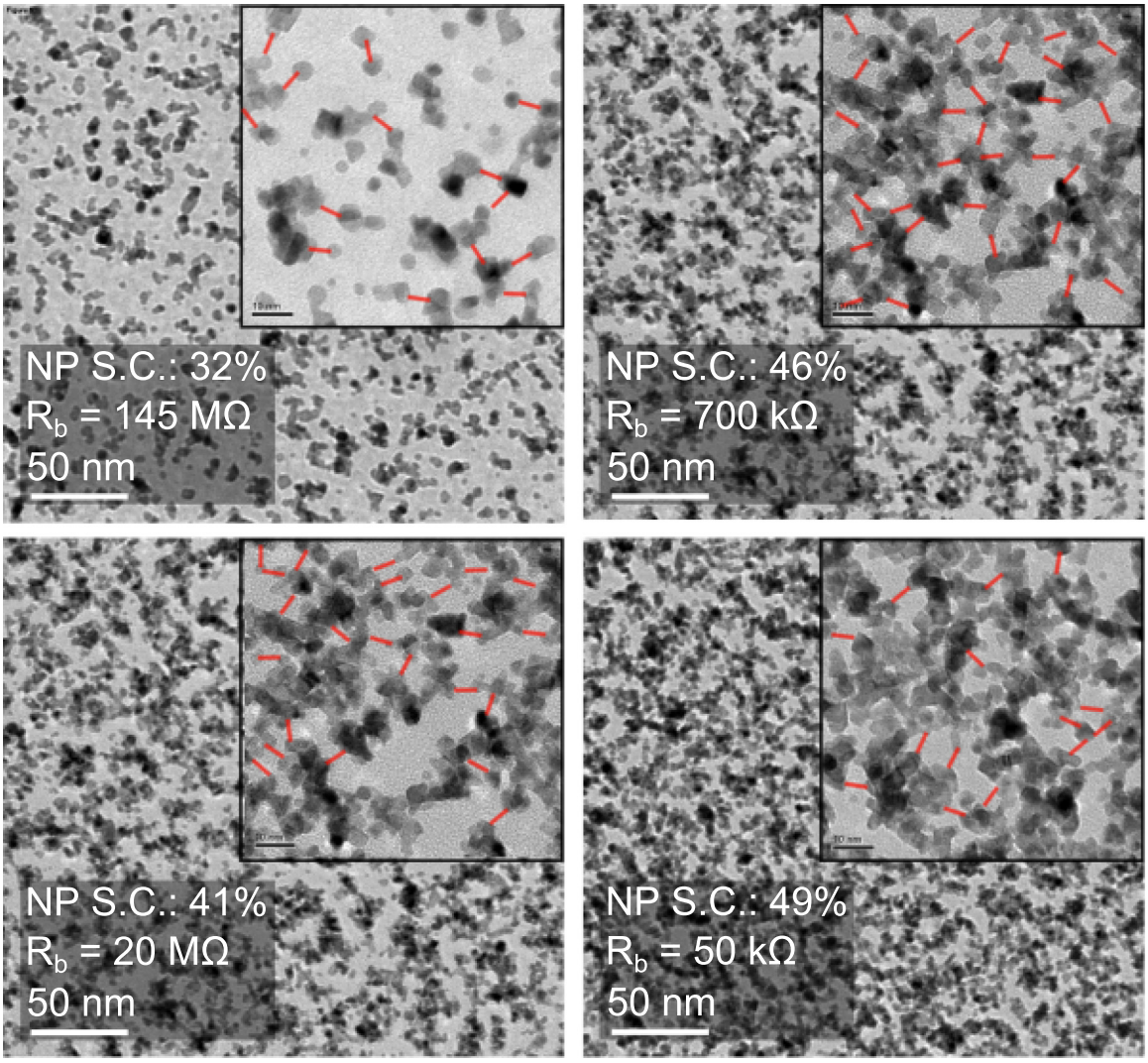

Fig. 5. TEM images for sensors of varying nanoparticle (NP) surface coverage (S.C.), as discussed in all of the above sensing experiments. Straight lines of 5 nm in length, mark areas within the nanoparticle film with an inter-nanoparticle distance equal or smaller than 5 nm.

sensors" (sensors modified with NC probe DNA) to target DNA hybridization is clearly distinguishable from that for sensors modified with FC probe DNA. A small response in $|\Delta R|/R_0$ of 4–8% has been observed throughout the experiments for all control sensors, for a NC DNA concentration of 10 μM (a small percentage of NC probe DNA is expected to non-specifically interact with target DNA). The mean sensor response to NC probe to target DNA hybridization (for a 10 μM concentration) was found to be around 5% throughout all of the sensing experiments.

3.2.2. Oligomer concentration saturation on the sensor surface, limit of detection (LOD) and detection of single base pair mismatched DNA

As a final step, the effect of probe DNA concentration on sensor response, the ability of the sensor to detect single base pair mismatches in probe to target DNA hybridization as well as the limit of detection of the device, were investigated. In all of the following experiments optimized nanoparticle biosensors have been solely used (surface coverage of 46% and an IDE gap of 5 μm).

The hybridization of the immobilized probe DNA with two different concentrations of target DNA (10 μM and 1 μM) produced two clearly distinguishable resistance shifts. Reduction of the amount of the immobilized probe ssDNA from 10 μM to just 1 μM revealed that the sensor's surface quickly becomes saturated with probe DNA. The response of the sensor for the reduced probe ssDNA concentration, resulted in an almost identical response with the one obtained when the surfaces were functionalized with 10 μM of probe ssDNA. Saturation of the sensor's surface with probe DNA is crucial for ensuring the detection of low concentrations of target DNA and can affect DNA hybridization efficiency, hence sensing response (Peterson et al., 2001).

In Fig. 4 the sensor's response can be seen for varying concentrations of target DNA. The sensor is able to detect the hybridization of FC probe to target DNA for target DNA as low as 1 nM in concentration while there is clear differentiation between FC DNA detection and single base pair mismatched DNA (The sensor systematically shows reduced response, in the range of 20–35%, when in the presence of single base pair mismatched DNA). It is worth noting that control experiments using NC probe DNA, for concentrations lower than 100 nM, resulted in undetectable changes in the resistance of the sensor. For each distinctive concentration of target DNA, 10 different optimized DNA biosensors have been used in order to ensure the reproducibility of the measurements. The standard deviation of these measurements varied from 1% to 3% as can be seen in Fig. 4.

3.2.3. Conductivity response to DNA hybridization

The increased performance offered by bio sensing devices having a resistance/conductivity that is close to the percolation

threshold can be connected to the structure of the nanoparticle film or, equivalently, to the number of charge transfer percolation paths available within the platinum nanoparticle layer. In this conductivity scenario the sensor is close to an "inflection point", as far as its conductivity is concerned, and DNA-mediated charge transport can assist the sensor to transcend from one conductivity state to the other. The sensor's intermediate conductivity state renders the charge transport within the nanoparticle film, extremely sensitive to any change in the nanoparticle surrounding medium (Eqs. (1) and (2)). The presence of hybridized DNA chains can induce a substantial shift in the resistance/conductivity of the nanoparticle-based device when these DNA chains act as conductive bridges between discrete nanoparticles or nanoparticles clusters, forming new high conductivity DNA-mediated charge transport/percolation pathways. In the case of sensors having a nanoparticle surface coverage that is higher than the optimal coverage of 46%, reduced sensitivity is to be expected. Sensors in the quasi macroscopic or metallic conductivity state in particular (nanoparticle surface coverage $>49\%$) present an already overwhelming amount of available nanoparticle charge transport pathways and the additional "conductive bridging" offered by the hybridized dsDNA chains has little or no effect to the overall conductivity of the sensor (Fig. 5). On the other hand if the nanoparticle surface coverage is suboptimal (smaller than 42%), reduced sensitivity is to be expected since the hybridized dsDNA chains cannot physically create as many DNA mediated charge pathways as in the optimized sensor. Sensors with conductivity that falls in the insulating regime (nanoparticle surface coverage $<32\%$) present nanoparticle aggregates that are widely separated from each other, with scarce or no charge transport pathways, that are unable to be "bridged" by the hybridized DNA chains (Fig. 5). Careful analysis of TEM images reveals that for sensors having an optimal nanoparticle surface coverage of 46%, "open" or yet unconnected inter-nanoparticle charge pathways are introduced (inter nanoparticle spacing of 5 nm, which is comparable to that of the hybridized DNA chains, as can be seen in Fig. 5).

The increased sensitivity offered in the case of sensors having conductivity close to the percolation threshold is ultimately a product of their critical surface density which leads to an intermediate transition conductivity state (the main cause of reduced sensing performance for increased nanoparticle surface coverage sensors) as well as to a fitting inter-nanoparticle distance (the main cause of reduced sensing performance for reduced nanoparticle surface coverage sensors).

4. Conclusions

The current study focused on the development and optimization of nanoparticle-based biosensors. The sputtering technique (employed for the production and self-assembly of the nanoparticle layer) allows facile and precise control over the nanoparticle surface coverage, in a room temperature environment, without the usual chemical modification required for nanoparticles. In addition, no chemical modification of the nanoparticle layer or of the substrate is required in order to tune the inter-nanoparticle distance.

By optimizing the design parameters of the biosensor (IDEs inter finger distance and nanoparticle surface coverage), fine-tuned biosensors have been produced. The optimal nanoparticle surface coverage has been confirmed to be again around 46%, just below the percolation threshold, where the structural and electrical properties of the nanoparticle layer offer increased sensing response.

The optimized biosensor prototype was proven to have a limit of detection (LOD) of 1 nM while the sensor has been able to successfully differentiate between FC and 1MM DNA, paving the way for the detection of inherent or acquired mutations of clinical significance. Furthermore, the fact that the inter-nanoparticle distance can be tuned in order to match the length of any hybridized DNA strands, (inter-nanoparticle distance can be modified via deposition time and DNA's length is proportional to the amount of base pairs) renders the proposed biosensor an extremely flexible device that can be tailored made to fit in a variety of bio-sensing scenarios. Its use can be expanded in the field of environmental monitoring, specific disease detection etc., while it can be easily integrated alongside chemical or strain sensing devices, forming a multi-purpose sensing platform.

Acknowledgements

This research has been financed by the "I.K.Y. Fellowships of Excellence for Postgraduate Studies in Greece – SIEMENS Program 2014-2016″, of the State Scholarships Foundation (I.K.Y.).

Appendix A. Supporting information

Supplementary data associated with this article can be found in the online version at http://dx.doi.org/10.1016/j.bios.2016.03.028.

References

Abeles, B., Sheng, P., Coutts, M., Arie, Y., 1975. Adv. Phys. 24, 407–461.
Ahn, J., Lee, T.H., Li, T., Heo, K., Hong, S., Ko, J., Kim, Y., Shin, Y., Kim, M.G., 2011. Biosens. Bioelectron. 26, 4690–4696.
Ancona, M.G., Snow, A.W., Foos, E.E., Kruppa, W., Bass, R., 2006. IEEE Sens. J. 6, 1403–1414.
Armistead, P.M., Thorp, H.H., 2002. Bioconjug. Chem. 13, 172–176.
Boon, E.M., Barton, J.K., 2002. Curr. Opin. Struct. Biol. 12, 320–329.
Boutopoulos, C., Touloupakis, E., Pezzotti, I., Giardi, M.T., Zergioti, I., 2011. Appl. Phys. Lett. 98, 093703.
Dekker, G., Ratner, M.A., 2001. Phys. World 14, 29–33.
Drummond, T.G., Hill, M.G., Barton, J.K., 2003. Nat. Biotechnol. 21, 1192–1197.
Fojta, M., Havran, L., Billova, S., Kostecka, P., Masarik, M., Kizek, R., 2003. Electroanalysis 15, 431–440.
Fang, C., Fan, Y., Kong, J., Gao, Z., Balasubramanian, N., 2008a. Anal. Chem. 80, 9387–9394.
Fang, C., Fan, Y., Kong, J., Gao, Z., Balasubramanian, N., 2008b. Appl. Phys. Lett. 92, 263108.
Furst, A.L., Hill, M.G., Barton, J.K., 2014. Polyhedron 84, 150–159.
Gao, Q., Zhang, W., Guo, Y., Qi, H., Zhang, C., 2011. Electrochem. Commun. 13, 335–337.
Giese, B, 2000. Acc. Chem. Res. 33, 631–636.
Kelley, S.O., Barton, J.K., Jackson, N.M., Hill, M.G., 1997. Bioconjug. Chem. 8, 31–37.
Kelley, S.O., Jackson, N.M., Hill, M.G., Barton, J.K., 1999. Angew. Chem. Int. Ed. 38, 941–945.
Lee, J.S., Ulmann, P.A., Han, M.S., Mirkin, C.A., 2008. Nano Lett. 8, 529–533.
Li, Z., Miao, X., Xing, K., Peng, X., Zhu, A., Ling, L., 2016. Biosens. Bioelectron. 80, 339–343.
Lin, X.H., Wu, P., Chen, W., Zhang, Y.F., Xi, X.H., 2007. Talanta 72, 468–471.
Ling, P., Lei, J., Jia, L., Ju, H., 2016. Chem. Commun. 52, 1226–1229.
Malecka, K., Stachyra, A., Góra-Sochacka, A., Radecka, H., Radecki, J., 2016. Sens. Actuator B-Chem. 224, 290–297.
Merkoçi, A., 2010. Biosens. Bioelectron. 26, 1164–1177.
Neugebauer, C.A., Webb, M.B., 1962. J. Appl. Phys. 33, 74–82.
Okahata, Y, Kobayashi, T, Tanaka, K, Shimomura, M, 1998. J. Am. Chem. Soc. 120, 6165–6166.
Palecek, E., 1960. Nature 188, 656–657.
Palecek, E., 1988. Anal. Biochem. 170, 421–431.
Palecek, E., Fojta, M., Jelen, F., 2002. Bioelectrochemistry 56, 85–90.
Peterson, A.W., Heaton, R.J., Georgiadis, R.M., 2001. Nucl. Acids Res. 29, 5163–5168.
Porath, D., Bezryadin, A., De Vries, S., Dekker, C., 2000. Nature 403, 635–638.
Qi, J., Govind, N., Anantram, M.P., 2015. J. Chem. Phys. 143, 094306.
Scher, H., Zallen, R., 1970. J. Chem. Phys. 53, 3759–3761.
Singhal, P., Kuhr, W.G., 1997. Anal. Chem. 69, 4828–4832.
Skotadis, E., Tanner, J.L., Stathopoulos, S., Tsouti, V., Tsoukalas, D., 2012. Sens. Actuator B-Chem. 175, 85–91.
Skotadis, E., Mousadakos, D., Katsabrokou, K., Stathopoulos, S., Tsoukalas, D., 2013. Sens. Actuator B-Chem. 189, 106–112.
Tanner, J.L., Mousadakos, D., Giannakopoulos, K., Skotadis, E., Tsoukalas, D., 2012.

Nanotechnology 23, 285501.
Tokonami, S., Shiigi, H., Nagaoka, T., 2008. Anal. Chem. 80, 8071–8075.
Tsekenis, G., Chatzipetrou, M., Tanner, J., Chatzandroulis, S., Thanos, D., Tsoukalas, D., Zergioti, I., 2012. Sens. Actuator B-Chem. 175, 123–131.
Umek, R.M., Lin, S.W., Vielmetter, J., Terbrueggen, R.H., Irvine, B., Yu, C.J., Kayyem, J. F., Yowanto, H., Blackburn, G.F., Farkas, D.H., Chen, Y.P., 2001. J. Mol. Diagn. 3, 74–84.
Wang, L., Kariuki, N.N., Schadt, M., Mott, D., Luo, J., Zhong, C., Shi, X., Zhang, C., Hao, W., Lu, S., Kim, N., Wang, J., 2006. Sensors 6, 667–679.
Wang, L., Shi, X., Kariuki, N.N., Schadt, M., Roger Wang, G., Rendeng, Q., Choi, J., Luo, J., Lu, S., Zhong, C.J., 2007. J. Am. Chem. Soc. 129, 2161–2170.
Wang, F., Yang, C., Duan, M., Tang, Y., Zhu, J., 2015. Biosens. Bioelectron. 74, 1022–1028.
Yang, I.V., Thorp, H.H., 2001. Anal. Chem. 73, 5316–5322.
Yang, I.V., Ropp, P.A., Thorp, H.H., 2002. Anal. Chem. 74, 347–354.